大韓土木學會論文集
第14卷 第4號 · 1994年 7月
pp. 703~710

極低사이클 荷重下에서 鋼部材의 損傷度評價를 위한 有限要素解析

Nonlinear FEM Analysis for Damage Assessment of Steel Members under Very-Low-Cycle Loading

朴 鍊 洙*
Park, Yeon Soo

Abstract

A nonlinear FEM analysis of steel members under very-low-cycle loading has been performed in conjunction with experimental works. This analysis is an FEM tracing toward cracking of steel members under cyclic loads such as a strong earthquake. After verifying the procedure by comparing global hysteretic behaviors from the analytical and experimental results, the local stress-strain hysteresis at critical sections for large cyclic deformations was traced by the numerical analysis. Local strain history was discussed in relation to cracking. Based on the experimental and analytical results, a new approach to seismic safety assessment for steel members was proposed in this paper.

要 旨

극저사이클 하중하에서 강구조부재의 비선형 유한요소해석을 실험과 더불어 수행하였다. 본 해석은 강진과 같은 반복하중하에서 강구조부재의 균열발생전까지를 유한요소법으로 추적한 것이다. 해석과 실험결과로부터 얻어진 히스테리틱 거동을 비교한 후, 큰 반복변형을 받는 응력집중부에 있어서 국소변형율의 이력을 수치해석에 의해 시뮬레이션하였다. 이 국소변형율의 이력과 극저사이클 파괴실험시의 균열발생 현상과의 관계를 정량적으로 분석하였다. 실험과 수치해석 결과를 바탕으로 강구조부재의 내진안전성 평가를 위한 새로운 방법이 본 논문에서 제시되었다.

1. Introduction

Damage process and its assessment of structural systems undergoing seismic excitations seem to be of great importance, since the social and economic effects of earthquake damage are quite significant. Structural damage and failure due to repeated large deformations such as strong earthquake are frequently attributed to plastic and/or unstable behavior of structures and their members. This has motivated the experimental investigations on failure of steel members due to very-low-cycles of loading,[1-3] which are herein meant to involve load repetitions of the order of five to twenty cycles. The experiments were executed up to occurrence of visible cracks or rupture of the angle members.

* 正會員 · 漢陽大學校 超大型構造시스템硏究센터 硏究助敎授, 工學博士

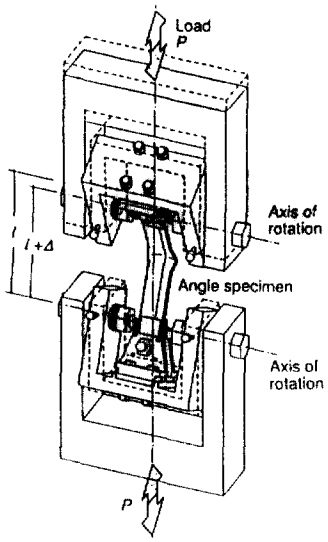

Fig. 1. Testing system

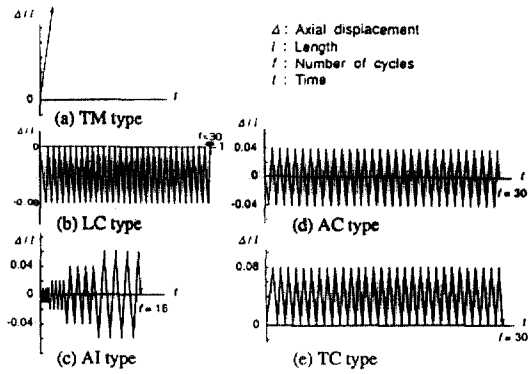

Fig. 2. Loading patterns

The purpose of this analysis is to simulate the hysteretic behavior of the tested angle specimens under such very-low-cycle loading and to trace the local stress-strain history at critical parts that cannot be observed through the experiments. The computer model is based on a three-dimensional, hysteretic analysis by using the finite element method (FEM), the MSC/NASTRAN program,[4-6] which includes the effects of the material and geometric nonlinearities. A total of six specimens selected from the experiments has been simulated in the analysis. This program does not include analyses for crack occurrence and/or crack propagation. However, the analysis is effective at least up to the number of loading cycles at which cracking was observed in the experiments. Then, it is considered that the process on outbreak of cracking for the steel members can be traced by this numerical method.

A new approach to seismic damage estimation of steel members was suggested herein. This method was based upon the experimental and numerical investigations for steel angle members under very-low-cycles of loading. Importance of the parameter, local strain, was discussed in relation to cracking to identify a quantitative relationship between damage and itself. The proposed damage estimation method was focused on the local strain history at the cross-section of the most severe concentration of local deformation.

2. Outline of Experimental Works

The experimental investigations were performed on steel angles. Two types of angles L-40×40×3 and L-40×40×5 made of the SS400 grade steel served as specimens. Each specimen was pin-supported, as indicated in Fig. 1. The effective length l between the pin-supports, being the tested part, was 318 mm, as shown in Table 1. A slowly varying uni-axial load was applied to near-centroid of the cross-section, using the hydraulic servo-actuator. Load was controlled by the relative axial displacement Δ. The choices of loading pattern were from monotonic elongation (TM type), constant displacement amplitude (LC, AC and TC types) and increased displacement amplitude (AI type), as shown in Fig. 2. In order to measure residual local strain after testing, the dot marking at 2 mm intervals in the direction parallel to the longitudinal axis for a mid-part length of 80 mm was made on the surface before testing, at the both edges and the corner in the cross-section of the specimen, using a Vickers hardness tester.

3. Experimental Results

Fig. 3 is a sketch of buckling deformation and visible cracks. During testing, the positive (P mode) or negative (N mode) deflection was observed, as defined in the figure. The global buckling

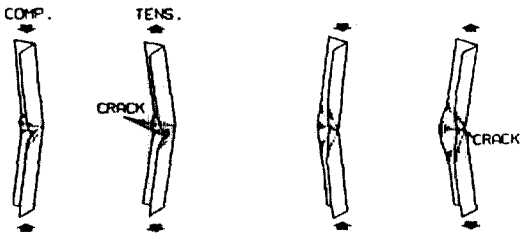

(a) P mode (b) N mode

Fig. 3. Deflection modes

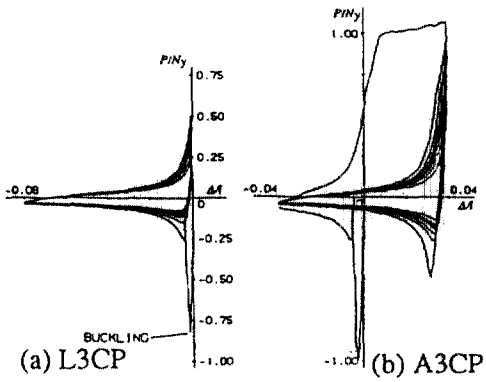

(a) L3CP (b) A3CP

Fig. 4. Load-axidal displacement relations (Experiment)

deflection was accompanied by significant localized deformation due to plate local buckling of the legs at the mid-part of the specimen, which induced very large strains. Typical examples of the observed load-axial displacement relationships are shown in Fig. 4. Here the load P and relative displacement Δ are normalized by the yield load N_y and length l, respectively.

The number of load cycles at three cracking states and rupture are listed for each specimens in Table 1. Irrespective of the loading patterns and deflection modes, visible cracks were initiated when stretching the concave-side surface of the overall or local bucking deformation induced in the preceding load cycles. Visible cracks at the convex side were observed within 1-4 cycles following the concave side cracking. Cracking on the concave and convex sides rapidly penetrated through the thickness of the legs.

Visible cracks were located near the regions of severe concentration of strains. The maximum absolute value of residual "net" strain, excluding contributions from the crack opening, at a visible crack portion was of magnitude of the order of 30~35% (see ε_{tens} and ε_{comp} in Table 1), independent of the test parameters; Whereas in the monotonic-tension test of T3M specimen (see Table 1) and in material test,[1-3] the maximum "net" local strain near the ruptured portion was about 100%. So those residual strain values are considered to reflect the effect of repeated loading.

Table 1. Specimen sizes, test parameters and test results (selected from Ref. 2)

Specimen name	Angle type	Length l (mm)	Width b (mm)	Thickness t (mm)	Loading pattern	Number of load cycles: Crack f_{cav}	Crack f_{vex}	Crack f_{pen}	Rupture f_{rup}	Strain at cracked part: ε_{tens}	ε_{comp}
T3M	L-40×40×3	316	39.7	2.97	TM	–	–	–	–	115%	–
L3CP	L-40×40×3	318	39.6	2.83	LC	5	8	8	23	30%	−32.5%
A3IP	L-40×40×3	316	39.7	2.98	AI	8	11	11	13	65%	−35%
A3CP	L-40×40×3	316	39.7	2.98	AC	4	7	8	17	35%	−30%
T3CP	L-40×40×3	316	39.7	2.97	TC	4	8	8	17	35%	−30%
T3CN	L-40×40×3	318	39.6	2.97	TC	6	8	8	–	–	−30%
L5CP	L-40×40×5	317	39.2	4.55	LC	9	12	12	19	30%	−32.5%

[Note] f_{cav}: Number of cycles at first cracking on the concave side of bending deformation, f_{vex}: Number of cycles at first cracking on the convex side of bednding deformation, f_{pen}: Number of cycles at penetration in direction of plate thickness, f_{rup}: Number of cycles at rupture, ε_{tens}: Maimum absolute value of local strain of tensile-bending side at cracked part, ε_{comp}: Maximum absolute value of local strain of compressive-bending side at cracked part.

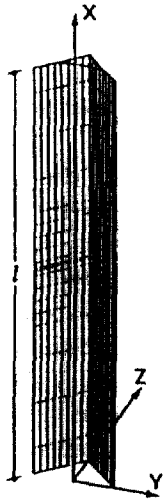

Fig. 5. Typical model (306 elements)

4. FEM Modeling and Loading

A typical finite element model for an angle specimen is shown in Fig. 5. The 4-noded quadrilateral isoparametric shell elements (QUAD4 elements) were used for modeling the tested angle specimen. The specimen was simply supported. The material property in this analysis has been assumed to be bilinearly elasto-plastic with kinematic hardening. The yield stress σ_y, Young's modulus E_s and Poisson's ratio ν were taken to be 349 N/mm^2, 2.06×10^5 N/mm^2 and 0.3, respectively. The slope E_t, in the strain hardening region of the stress-strain curve was selected as 1% of E_s. The von Mises yield criterion was used.

The model in this analysis had 306 shell elements and 1628 degress of freedom. In the model, only in-plane rotation was constrained in all the nodes of each shell elements. Table 2 is a summary of the analyzed cases. The analyzed models were subjected to cyclic enforced axial displacement, similarly to the experiment. In order to produce a desired deflection mode indicated in Fig. 6, the load was applied with small eccentricities distant from the centroid of each end cross-section in the Z-direction (see Fig. 5 and Table 2), also similarly to the experiment. The analysis was basically performed up to the prescribed number of cycles (Table 2) where outbreak and/or penetration of cracks were observed in the experiment. All computer runs have been made on the FUJITSU M-1800/30 system of Data Processing Center, Kyoto University. The analysis for each model took approximately 3 to 7 hours of CPU time.

5. Load-Axial Displacement Relations

A comparison is made between Figs. 4 and 7 for typical load-axial displacement curves from the experiment and analysis. The overall deformed shapes and load-axial displacement relations from the numerical analysis showed good agreement with those from the experiment, indicating the validity of the numerical results. In the case of loading started from the contraction side (see L3 CP in Figs. 4 and 7), the compressive load decreased suddenly after the global buckling taking place at an early stage of the first cycle, accompanied by the inelastic local buckling. Here one cycle is defined with reference to the load P. The compressive load-carrying capacities at each cycle after

Table 2. Analyzed cases and results

Model name	Loading pattern	Eccentricity e (mm)	Analyzed number of cycles	Local strainat at cracking stage ε_{tens} (%)	ε_{comp} (%)
L3CP	LC	−0.5	8	24.8	−26.5
A3IP	AI	−0.2	8	25.7	−15.0
A3CP	AC	−0.2	8	33.1	−21.3
T3CP	TC	1.0	8	36.5	−
T3CN	TC	−0.5	8	26.2	−
L5CP	LC	−0.5	12	21.6	−29.5

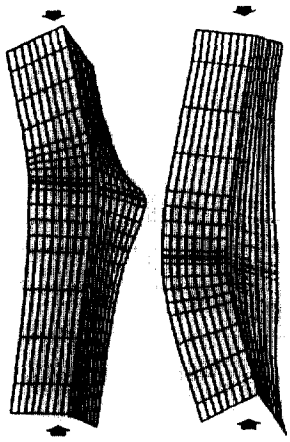

(a) P mode (b) N mode

Fig. 6. Deformed shapes at $\Delta/l=-0.08$

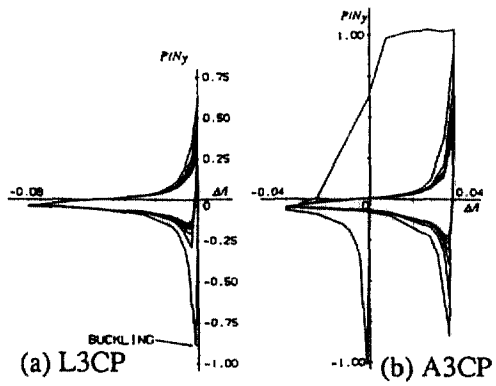

Fig. 7. Load-axial displacement relations (Analysis)

the first cycle were significantly reduced, but relatively a small decrease was seen in the succeeding tensile load-carrying capacities. A fairly higher compressive strength in the second cycle in the case of the alternately constant displacement loading (A3CP) was calculated from the numerical analysis. This phenomenon may be attributed to the fact that a nearly straight configuration was regained by purely tensile yielding from a crooked configuration in the contraction range.

6. Longitudinal Distribution of Local Strain

Longitudinal-strain distribution caused by local

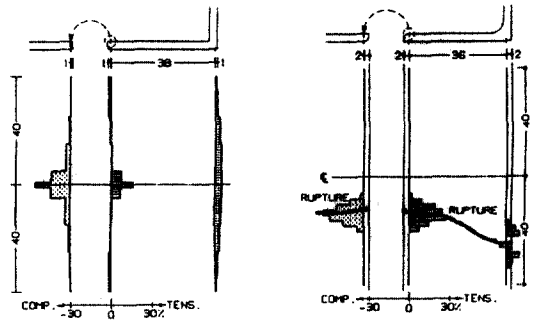

Fig. 8. Local strain distribution at $\Delta/l=-0.08$ (L3CP)

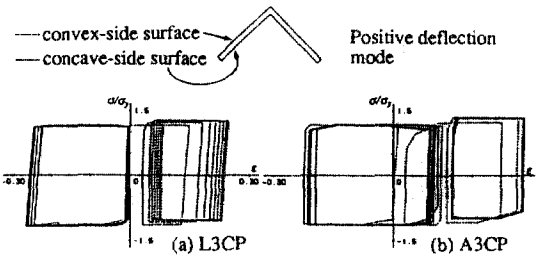

Fig. 9. Local stress-strain hysteresis

buckling induced very large local strains at the mid-critical portion of models. Fig. 8(a) presents the axial strain on the edge and corner surfaces, along the longitudinal direction at a mid-part length of 80 mm for L3CP, calculated by the analysis in the loading cycle, where the visible crack was observed in the experiments. This behavior agreed well with the measured distribution of residual strains of test specimens (see Fig. 8(b)). The maximum absolute values of strains in the cracking stages were of the order of 20~40% at both compressive- and tensile-bending sides, as shown in Fig. 8 and Table 2, irrespective of the analysis cases. These values correspond to the maximum values of residual "net" strains at the cracked portion under the very-low-cycle loading experiments.[1-3]

7. Simulation of Local Stress-Strain Hysteresis

Fig. 9 shows the typical axial stress-strain hys-

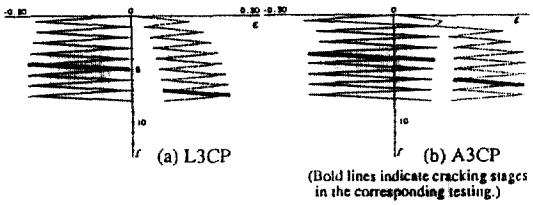

Fig. 10. Local strain histories with the increasing number of cycles

teresis on the extreme-fibers of the concave and convex sides of the bending deformation at the edge element of the mid-height cross-section. Fig. 10 shows the corresponding strain history with increasing number of cycles. Regardless of the loading patterns, the strain amplitude (i.e. the variable width) on the concave-side surface is larger than that on the convex-side surface. This means that the most severe cycling of local strain occurs at the concave-side surface of the global and/or local buckling deformation. The outbreak of a crack observed in the experiment is indicated by bold lines in Fig. 10. This can be related to the experimental phenomenon of the first cracking on the concave-side surface of the buckling deformation.

A computation was made for the summation of plastic components of strain in the tensile stress side in each cycle, up to the cycle at the outbreak of cracks observed from the experiments. This attained the values of 104% to 255% through the simulated cases. These values seem to have correlation with the residual local strain of 90% to 115% at the ruptured portion under the previously mentioned monotonic-tension test. This sum might be an indicator to represent cracking due to the accumulated damage under very-low-cycle loading.

8. Seismic Damage Assessment for Structural Steel Members

Fig. 11 presents the relations between the summation of local strain in the critical cross-section and the increasing number of cycles for all the models obtained from the analysis. Here the lower and upper dash lines correspond to 90% and 115%

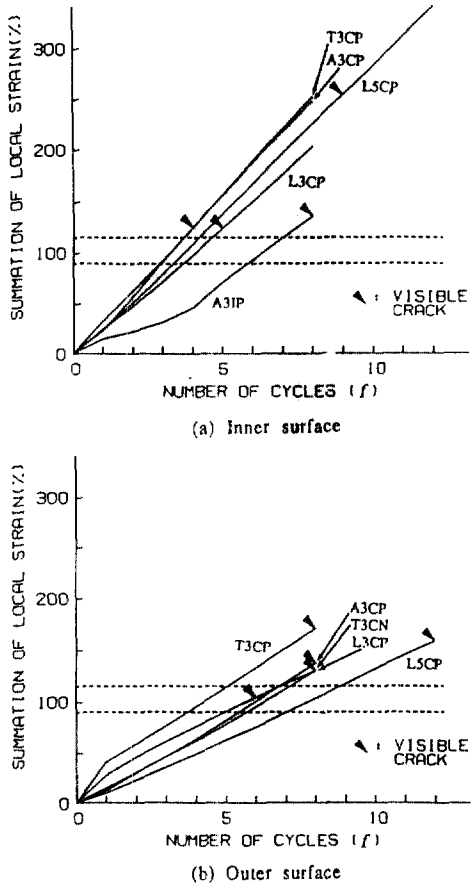

Fig. 11. Relationships between the summation of local strain and the increasing number of cycles

of the residual local strain at the ruptured portion under monotonic-tensile testing, respectively. The new method may be described by the summation of the critical local strain in the course of increasing number of cycles, which is conservatively compared with the threshold value 90% of the local strain at the ruptured portion under the monotonic-tensile testing. That is, the failure state is indicated if the summation of the local strain in the critical cross-section exceeds the limit strain of 90%.

Thus, the damage indicator under cyclic excitations as in strong earthquakes may be formulated as follows;

$$\text{If } \sum_{i=1}^{N} \varepsilon_i \geq \varepsilon_{limit}, \text{ then failure state} \qquad (1)$$

and

$$\text{If} \quad \sum_{i=1}^{N} \varepsilon_i < \varepsilon_{limit}, \text{ then no failure} \qquad (2)$$

where N, ε and ε_{limit} are the number of cycles, the local strain in the critical cross-section and the limit strain, respectively. The value of ε_{limit} might be 90% in the case of structural steel membres under the very-low-cycle loading. In general, the finite element analysis with material nonlinear and geometric nonlinear effects yields one of the most accurate prediction for the local strain history. The strain history may be calculated by the numerical approach as described in the above numerical analysis.

From Eqs. (1) and (2), the damage "D" of steel member to "N" cycles can be determined by the normalized form as follows;

$$D = \sum_{i=1}^{N} \left(\frac{\varepsilon_i}{\varepsilon_{limit}} \right) \qquad (3)$$

Therefore, $D \geq 1$ indicates the failure state, while $D < 1$ denotes a degree of damage at the corresponding loading step. For future research, however, the analytical and experimental investigations for structural steel members having various shapes under very-low-cycle loading are needed to verify the damage indicator of the above equation.

9. Conclusions

Based on this study of steel members under very-low-cycle loading, the following conclusions can be deduced:

1) The significance of finite element analysis has been established in the description of local behavior and the step-by-step tracing of elasto-plastic behavior for steel members under severe cyclic deformations in the post-buckling range. The overall deformed shapes and load-axial displacement relations from the numerical analyssis showed good agreement with those from the experiment, indicating the validity of the numerical results.

2) Longitudinal-strain distribution caused by bucking induced very large local strains at the mid-critical portion of the model. This behavior agreed well with the measured distribution of residual strains of test specimens. The maximum absolute values of strains at the cracking cycle were of the order of 20~40% at both compressive- and tensile-bending sides, irrespective of the analysis cases. These values corresponded to the maximum values of residual "net" strains at the cracked portion under the very-low-cycle loading experiments.

3) The local stress-strain hysteretic behavior at the critical section was traced by the numerical analysis. The most severe strain-cycling occurs on the concave-side surface of the globel and/or local buckling deformation. This can be related to the experimental phenomenon of the first cracking on the concave-side surface of the buckling deformation.

4) Up to the cycle at the outbreak of cracks observed from the experiments, a computation was made for the summation of plastic components of the strain in each cycle. This value was in a range of 104~255% in the simulated cases. These results were related to the residual local strain of 90~115% at the ruptured portion under the monotonic-tension test. It is possible that the local strain might give an information to evaluate cracking due to the cumulative damage of steel members under very-low-cycle loading.

5) A new approach to seismic damage assessment for steel members has been proposed in conjunction with the experimental numerical investigations. The new damage estimation method might be described by the summation of the critical local strain in the course of increasing number of cycles, which is compared with the threshold value 90% of the residual local strain at the ruptured portion under the monotoic-testing. Thus, this new method might enable the damage estimation for failure as well as in intermediate damage states.

References

1. Park, Y.-S., Iwai, S., Nonaka, T., and Kameda, H., "Tests on Failure of Angles under Very Low Cycles of Loading", *Proc. of the 1st KAIST-National Taiwan Univ.-Kyoto Univ. Tri-lateral Seminar/Wor-*

kshop on Civil Engineering, Kyoto, Japan, 1991, pp. 53-56.
2. Park, Y.-S., Iwai, S., Nonaka, T., and Kameda, H., "Experimental Study on Structural Failure of Steel Angle Members due to Very Low Cycle Fatigue under Earthquake Loading", *Proc. of the 21st JSCE Earthquake Engineering Symposium,* Japan Society of Civil Engineers, No. 125, Tokyo, Japan, 1991, pp. 481-484.
3. Iwai, S., Park, Y.-S., Nonaka, T., and Kameda, H., "Very Low-Cycle Fatigue Tests of Steel Angles", *Jour. of Structural and Construction Engineering,* AIJ, No. 445, 1993, pp. 139-149 (in Japanese).
4. MSC/NASTRAN, *Application Manual,* The Macneal-Schwendler Co., Los Angels, California, 1983.
5. MSC/NASTRAN, *User's Manual Vol. I & II,* The Macneal-Schwendler Co., Los Angels, California, 1985.
6. MSC/NASTRAN, *Handbook for Nonlinear Analysis,* The Macneal-Schwendler Co., Los Angeles, California, 1992.

(接受 : 1993. 10. 5)